

NUMERICAL STUDY ON THE INFLUENCING MECHANISM OF TWISTED RATIO IN OUTWARD CONVEX CORRUGATED TUBES WITH A TWISTED TAPE INSERT

by

Huaizhi HAN, Longbin YANG^{*}, Yiran HU, Ruitian YU, and Qun ZHANG

College of Power and Energy Engineering, Harbin Engineering University, Harbin, China

Original scientific paper
<https://doi.org/10.2298/TSCI170614042H>

Numerical investigations were conducted on flow and heat transfer in an outward convex corrugated tube with various structural twisted tape inserts. The study investigated the influence of twisted ratio on thermodynamic regulation and mechanism in the corrugated tube. The results indicate that Nusselt number in the corrugated tube (Nu_c) exceeds those in the corrugated tube and smooth tube by 120-136% and 171-317%, respectively. Meanwhile, the friction factor increases by 148-153% and 476-514%, respectively. The best overall thermal performance ($\eta = 1.97$) is obtained with a high twist ratio ($y/w = 5$). However, the highest thermal performance ($Nu_c/Nu_s = 4.78$) is obtained with the lowest twist ratio ($y/w = 1.25$).

Key words: corrugated tube, twisted tape insert, heat transfer enhancement, numerical simulation

Introduction

Heat exchangers are widely used in almost every field of engineering including chemical industries, petroleum refineries, power engineering, mechanical engineering, automobile, cryogenic, aerospace, electronics. Therefore, improving heat exchangers to obtain high heat transfer performance is considered as significant research aspects. Several heat transfer augmentation techniques are adopted to enhance the heat transfer performance of heat exchanger, which makes reduction in size and operating costs.

Heat transfer augmentation techniques can be divided into three categories, including active methods [1-3], passive methods [4-6], and compound methods, respectively. Among these methods, compound methods are able to enormously enhance the heat transfer according to use two or more methods simultaneously. This is also termed as a fourth-generation heat transfer technology. It should be noted that the compound method accommodates further development of heat transfer augmentation techniques, which exceeds any of the fore-mentioned techniques acting independently. Compound methods owe several combinations, passive-passive ones attract increasing attention from researchers and engineers due to the ease of use and low cost.

With respect to passive compound methods in a single-phase flow, most of the research efforts were devoted toward various surface rough wall configurations combined with twisted tape inserts. Extant researches focus on these types of tubes, which are performed in the

^{*}Corresponding author, e-mail: ylbhrb@163.com

laminar and turbulence flow regime by means of experiments. Van Rooyen and Kroeger [7] experimentally investigated thermodynamic performance of laminar oil flowing in internally finned tubes with twisted-tape inserts under a constant wall temperature. Pramanik and Saha [8] experimentally studied thermodynamic characteristics of laminar oil through ducts with internal transverse rib. Bharadwaj *et al.* [9] experimentally investigated thermodynamic characteristics in a 75-start spirally grooved tube with a twisted tape insert with water medium. Liao and Xin [10] conducted experimental study on thermodynamic characteristics of three types of heat transfer mediums in four types of internal extended surface tubes combined with two types of insert structures. Promvonge and Eiamsa-ard [11] experimentally researched heat transfer, resistance, and overall heat transfer characteristics of a round tube combined with conical-ring and twisted tape swirl generator structures for fully developed turbulence. Hong *et al.* [12] conducted experiments to investigate compound thermodynamic characteristics of a converging-diverging tube combined with a twisted tape insert in a fully developed flow regime. Thianpong *et al.* [13] experimentally examined compound heat transfer and resistance behavior of air with fully developed turbulent regime in a dimpled tube that was combined with a twisted tape.

Extensive experimental studies investigated a rough surface tube coupled with various twisted inserts. However, only a few studies examined the compound technique by numerical methods. A previous study demonstrated that the augmentation of heat transfer in the shellside of an outward convex corrugated tube significantly is much larger than in the tubeside [6]. According to the fundament of increasing heat transfer coefficient, it is necessary to adopt methods to enhance heat transfer in the tubeside. Thus, the present study adopts an outward convex corrugated tube combined with a twisted tape (CT) as a new type of passive compound method to perform a numerical investigation. The thermodynamic performance and synergistic effecting flow and heat transfer mechanism for CT will be investigated in this research work.

Physical models

The geometries of the CT and a conventional smooth tube with a twisted tape (ST) are depicted in fig. 1. The diameter of the tubes, D , corresponds to 20 mm, which is equal to the twisted width, w . The 180 twist pitch, y , with three different values is given as an effect factor. Therefore, various twist ratios with three values, $y/w = 1.5, 2.5, 5$, are adopted in the study. It is considered that the diameters of the ST are identical to that of the CT to investigate the compari-

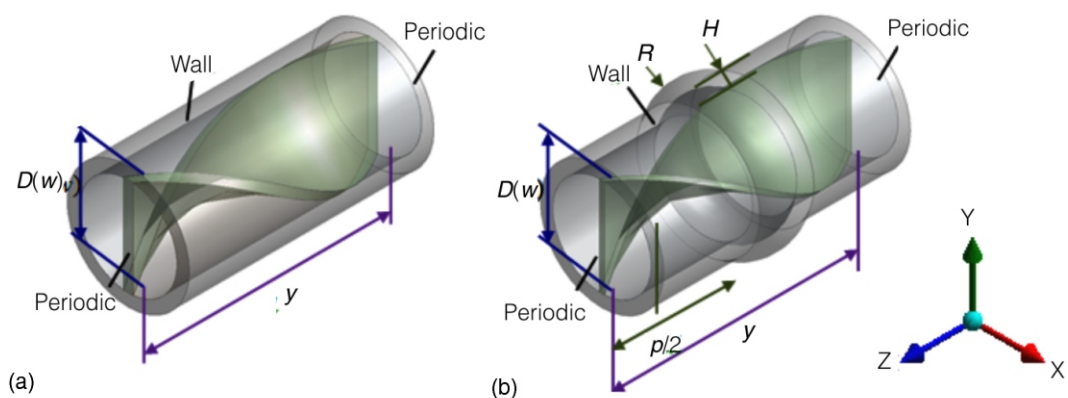


Figure 1. Physical model of the (a) ST and (b) CT

son between ST and CT. Compared with ST, an additional corrugated structure exist at the tube wall in the CT. The corrugated structural parameters include corrugation height, corrugation pitch, and corrugation crest radius that are fixed at $H = 1$ mm, $p = 50$ mm, and $R = 6$ mm, respectively.

Numerical details

Governing equations

The working fluid selected for the simulation is water with constant physical properties. A 3-D steady RANS method is adopted for numerical model, neglecting the effect of gravity and heat radiation.

The governing equations are:

– continuity equation:

$$\frac{\partial(\rho u_i)}{\partial x_i} = 0 \quad (1)$$

– momentum equation:

$$\frac{\partial}{\partial x_j}(\rho u_j u_j) = \frac{\partial P}{\partial x_i} - \frac{\partial}{\partial x_j} \left(\mu \frac{\partial u_i}{\partial x_j} + \frac{\partial u_j}{\partial x_i} - \frac{2}{3} \delta_{ij} \frac{\partial u_k}{\partial x_k} \right) - \frac{\partial}{\partial x_j}(\overline{\rho u_i u_j}) \quad (2)$$

The Boussinesq hypothesis is a common method to describe Reynolds stresses:

$$\overline{\rho u_i u_j} = \mu_t \left(\frac{\partial u_i}{\partial x_j} + \frac{\partial u_j}{\partial x_i} - \frac{2}{3} \rho k \frac{\partial u_k}{\partial x_k} \right) \delta_{ij} \quad (3)$$

and its corresponding energy equation is:

$$\frac{\partial}{\partial x_j} [u_j (\rho E - P)] = \frac{\partial}{\partial x_j} \left(\lambda_{\text{eff}} \frac{\partial T}{\partial x_j} \right) \quad (4)$$

The present study uses the RNG $k-\varepsilon$ turbulence model developed by Yakhot and Orszag [14] for the numerical simulation:

$$\frac{\partial}{\partial x_i}(\rho k u_i) = \frac{\partial}{\partial x_i} (\alpha_k \mu_{\text{eff}}) \frac{\partial k}{\partial x_j} - G_k - \rho \varepsilon \quad (5)$$

$$\frac{\partial}{\partial x_i}(\rho \varepsilon u_i) = \frac{\partial}{\partial x_j} (\alpha_\varepsilon \mu_{\text{eff}}) \frac{\partial \varepsilon}{\partial x_j} - \frac{C_{1\varepsilon}}{k} (G_k) - C_{2\varepsilon} \rho \frac{\varepsilon^2}{k} \quad (6)$$

where μ_{eff} denotes the effective viscosity, defined by $\mu_{\text{eff}} = \mu + \mu_t = \mu + \rho C_\mu k^2 / \varepsilon$, and the constants in the model include $C_\mu = 0.0845$, $C_1 = 1.42$, $C_2 = 1.68$, and $\alpha_k = \alpha_\varepsilon = 1.393$. It should be noted that $G_k = \rho u_i u_j (\partial u_j / \partial x_i)$ represents the generation of turbulent kinetic energy resulting from mean velocity gradients.

Initial and boundary conditions

A no-slip boundary condition is adopted on the wall surfaces of the tube and twisted tape. The constant boundary temperature 310 K are adopted on the outer tube wall and the inlet temperature are 300 K, respectively. Periodical boundary conditions are imposed at the inlet and

outlet of the physical model. In these conditions, the flow regime is fully developed. The periodical change of velocity, pressure, and temperature gradient within the domain:

$$u(r) \quad u(r-L) \quad u(r-2L) \quad \dots \quad (7)$$

$$\Delta P \quad P(r) \quad P(r-L) \quad P(r-2L) \quad P(r-3L) \quad \dots \quad (8)$$

$$\Theta \quad \frac{T(r-L) - T(r)}{L} \quad \frac{T(r-2L) - T(r-L)}{L} \quad \dots \quad (9)$$

Here, the variable quantities u , P , Θ , r , and L represent velocity, local pressure drop, temperature gradient, position vector, and periodic length vector, respectively. The Reynolds numbers imposed on the tube inlet correspond to 3000, 4000, 6000, 8000, and 10000 in the transition region.

Numerical procedure

The commercial software, ANSYS FLUENT 13.0, is selected as the CFD tool. The finite volume method was applied to discretize the governing equations, and the steady-state implicit format was adopted to solve the equations. The velocity-pressure coupling is solved by using the SIMPLE algorithm. Standard pressure and second order upwind schemes are employed to discretize the momentum and energy equations in the numerical model. Furthermore, the convergence criterion was set to a 10^{-6} relative error for the energy of the system, and to a 10^{-4} relative error for all other variables.

Grid independent analysis

The computational domain for the ST is resolved using non-structural elements. The pattern is limited to a single 180° twist length due to the periodic flow. A grid-independent solution for the ST is obtained by comparing the solutions from using different grid levels. The number of elements used for the simulation at each of the different grid levels approximately corresponds to 131743, 360304, 559507, 943241, and 1265716 elements. The errors from using the other four grid numbers when compared to the best grid number ($mn = 1265716$) increase monotonically in the following sequence when the number of elements decreases: 0.9%, 2%, 6%, and 14.2%. Therefore, the number of elements ($mn = 559507$) is selected as the optimal computational ST model, considering both convergence time and solution precision.

Figure 2 exhibits the verification by comparison between the numerical results and the experimental results obtained by Manglik and Bergles [15] under the same operating conditions. It could be found that the deviation between the numerical and experimental results is tiny. Therefore, the numerical model is accurate to calculate in this condition.

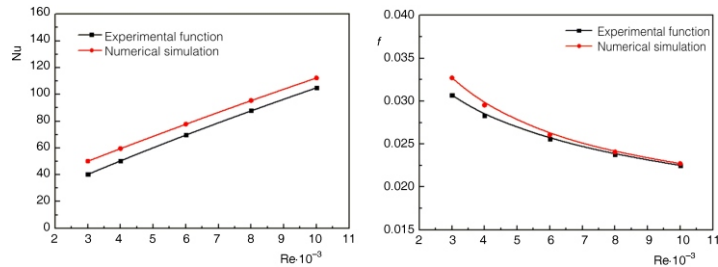
Results and discussion

Performance criteria

The Nusselt number can be calculated by:

$$\text{Nu} = \frac{\alpha D}{\lambda} \quad (10)$$

Figure 2. Comparison between numerical simulation and experimental function



where D is the characteristic diameter and the thermal conductivity λ is calculated from the fluid properties at the local mean bulk fluid temperature.

Friction factor, f , can be written as:

$$f = \frac{\Delta P}{\frac{L}{D} \frac{\rho u^2}{2}} \quad (11)$$

where ΔP is the pressure drop in experimental section, and L – the length of heat exchange tube.

The overall heat transfer performance, η , is used to evaluate the comprehensive performance of enhanced tube, which is defined:

$$\eta = \frac{\frac{Nu_c}{Nu_s}}{\frac{f_c}{f_s}^{1/3}} \quad (12)$$

The overall heat transfer coefficient $\eta > 1$ indicates the CT is superior to the ST. Otherwise, the enhanced heat transfer component is inferior to the ST.

Effect of twist ratio on heat transfer performance in CT

This section discusses the effect of twist ratio (y/w) on heat transfer, resistance, and overall heat transfer performance in the CT.

Figure 3(a) depicts the changing in Nusselt number ratio (Nu_c/Nu_s) with respect to Reynolds number with variations in y/w . The figure clearly illustrates that Nu_c/Nu_s tends to decline when Reynolds number increases. At similar operating conditions, Nusselt number in corrugated tube, Nu_c is 2.15-4.78 times higher than Nusselt number in smooth tube, Nu_s , which signifies the thermal performance of the CT is much superior than that of the ST. Moreover, the heat transfer improvement is more efficient at lower Reynolds numbers, owing to the thicker temperature boundary-layer. Additionally, Nu_c with $y/w = 1.25$ exceeds those with $y/w = 2.5$ and 5.0 by approximately 26-51% and 30-59%, which indicates the thermal performance is advantaged with the lower twisted ratio for the CT. The changing regularity of friction factor ratio, f_c/f_s , with various y/w is also shown in fig. 3(a). It is observed that f_c/f_s keep almost constant along with the changing Reynolds number, owing to the almost same increasing rate between the CT and the ST. The f_c/f_s evidently increases with the decreasing y/w , especially intense from $y/w = 1.25$ to $y/w = 2.5$, caused by larger turbulence intensity with shorter twist pitch. According to the figure, the friction factors generated by the compound devices with the twist ratios of $y/w = 1.25, 2.5,$ and 5.0 are approximately 15.68-16.22, 4.76-5.14, and 2.98-3.57 times than that of the ST, respectively.

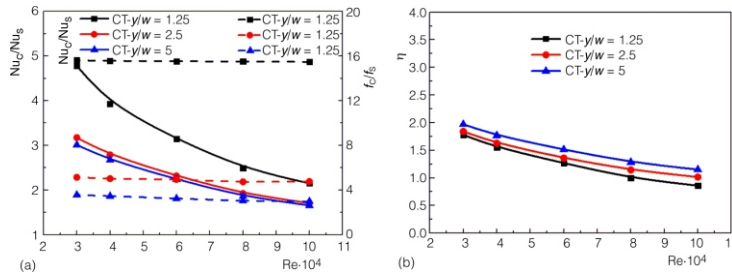


Figure 3. Effect of the twist ratio on flow and heat transfer performance

The synergistic effect of applying the corrugation combined with twisted tape on overall heat transfer performance, η , is presented in fig. 3(b). It could be seen from this figure, η exceeds unity ($\eta > 1$) for all enhancement devices under the condition of $Re < 8000$. This signifies a beneficial gain from the view of higher efficiency in the CT enhancements over that of a ST at almost Reynolds number range. Additionally, η decreases monotonously with the increasing of Reynolds number, indicating that the resistance performance increases faster than heat transfer performance. The data also presents a higher overall heat transfer performance with the increasing of y/w , which is attributed to the resistance performance increases faster than heat transfer performance with decreasing in y/w . A maximum $\eta = 1.97$ for the compound enhancement devices is observed at the lowest $Re = 3000$ and highest $y/w = 5.0$.

Effect of twist ratios on flow structure performance in CT

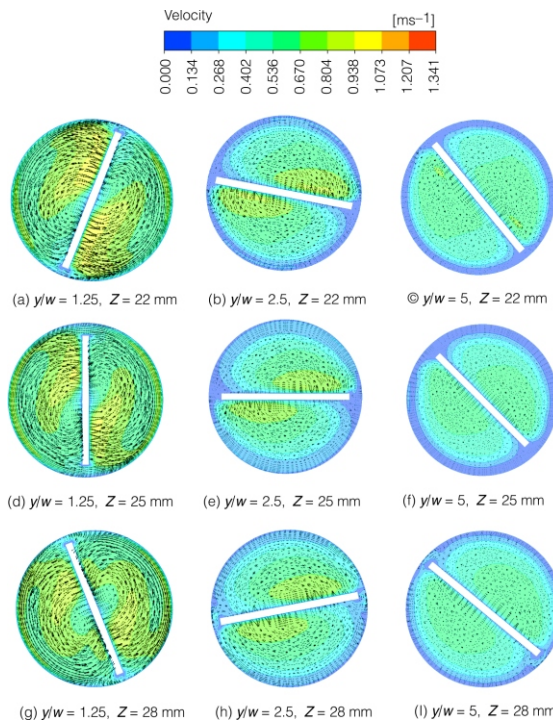


Figure 4. Velocity vector distribution with respect to various twist ratios

In order to capture the flow structure differences with various twist ratios along the channel of CT, a corrugation is divided into three different profiles (the positions of the three profiles are located at $Z = 22$ mm, 25 mm, and 28 mm, respectively). The velocity and temperature distribution at three profiles with various twisted ratios in CT are shown in figs. 4 and 5.

The prediction of the velocity vector for CT with various twist ratios at $Z = 22$ mm, 25 mm, and 28 mm are depicted in fig. 4. As shown in the figures, two types of secondary flow are produced in the tube. The first kind of secondary flow corresponds to a shed vortex flow adjoining the tube wall, which demonstrates that the reversed flow grows in the gap region between the corrugation and the margin of the twisted tape. Conversely, the second kind of swirl flow arising from the twisted tape improves fluid blending between the core region and the approaching tube wall region. The simultaneously generated transverse vortices from the corrugation structure and the longitudi-

nal vortices from the twin twisted tapes in the CT improve the heat transfer rate. It is also observed in the figures that two secondary flows are generated on both sides of the tape in the core flow area at $y/w = 1.25$. However, a secondary flow is absent at the other two ratios corresponding to $y/w = 2.5$ and 5. Additionally, the sizes of the arrows indicate that the velocity magnitude is maximum at $y/w = 1.25$ and evidently exceeds those at $y/w = 2.5$ and 5. Velocity distributions at various profiles are also displayed in this figure. At $Z = 22$ mm, the boundary-layer start to separate into wall boundary-layer and shear layer, because the tube wall begins to bend from the straight segment along the flow direction. Subsequently, at $Z = 25$ mm, an obvious swirl can be observed because the separated boundary-layer enclose a vortex and this profile located at the middle of the vortex. Finally, at $Z = 28$ mm, the separated boundary-layer will arrive the reattachment point near the corrugation trough.

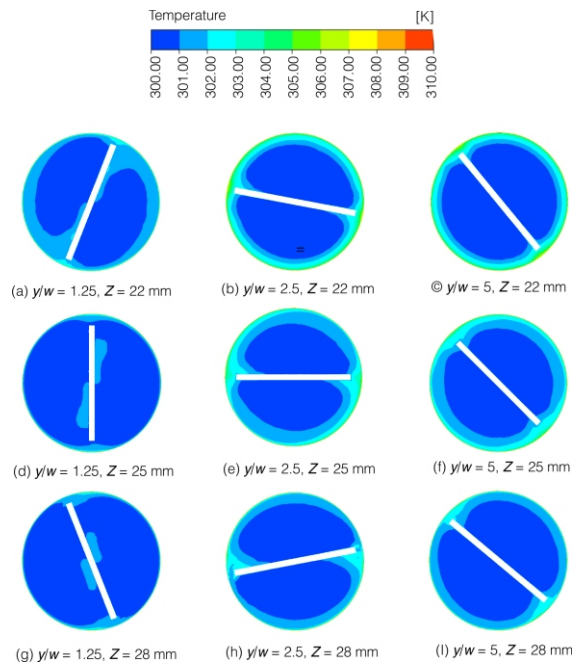


Figure 5. Temperature distribution with respect to various twist ratios

Figure 5 displays the contour plots of the temperature distributions for CT with various twist ratios at $Z = 22$ mm, 25 mm, and 28 mm. With respect to the three twisted tape structures, the $y/w = 1.25$ ratio exhibits a thinner boundary-layer when compared to the $y/w = 2.5$ and 5 twisted tapes for the same corrugation structure. This phenomenon is caused by increased sufficient mixing inside the CT with $y/w = 1.25$, which is caused by the reversed flow adjoining the tube wall and the swirl flow appearing in the core area. However, thermal boundary-layers in the radial direction are noticeably thicker due to poorer mixing in the tube with larger twist ratios, and this can be attributed to the lower intensity of swirl flow and the disappearance of the reversed flow. In this figure, the comparison of temperature distributions at the three profiles is also displayed. Due to the developing of thermal boundary-layer, the temperature boundary-layer is thicker at $Z = 22$ mm. Subsequently, the temperature boundary-layer becomes thinner at $Z = 25$ mm. Finally, the thinnest temperature boundary-layer occurs at $Z = 28$ mm.

Conclusion

In this study, a numerical simulation was performed to investigate the heat transfer and flow characteristics of CT and ST with respect to various twist ratios in a transition flow. The obtained results demonstrate that the best overall heat transfer performance ($\eta = 1.97$) exhibit in the CT with $y/w = 5$. Attaining the purpose of obtaining maximal heat transfer rate enhancement, it is necessary to consider CT with a low twist ratio ($y/w = 1.25$). The mechanism of compound heat transfer enhancement was further investigated by presenting the contour plots of significant physical quantities. The transverse vortices from the corrugation structure and the longitudinal vortices from twisted tapes are simultaneously imposed in a CT to enhance heat transfer rate. Furthermore, temperature gradient with respect to $y/w = 1.25$ is obvious larger than $y/w = 2.5$ and 5, meaning that the heat transfer performance is higher when $y/w = 1.25$.

Nomenclature

D	– hydraulic diameter, [m]
E	– total energy in eq. (4)
f	– fanning friction factor, [–]
H	– corrugation height, [m]
k	– turbulence kinetic energy, [m^2s^{-2}]
Nu	– Nusselt number, [–]
P	– pressure, [Pa]
p	– corrugation pitch, [m]
R	– corrugation crest radius, [m]
r	– position vector
Re	– Reynolds number, [–]
T	– temperature, [K]
u	– velocity, [ms^{-1}]
w	– twisted width
y	– twisted ratios

Greek symbols

α	– convective heat transfer coefficient, [$\text{WK}^{-1}\text{m}^{-2}$]
ε	– turbulence dissipation rate, [m^3s^{-2}]
l	– thermal conductivity, [$\text{WK}^{-1}\text{m}^{-2}$]
μ	– dynamic viscosity, [$\text{Kgm}^{-1}\text{s}^{-1}$]
ρ	– density, [Kgm^{-3}]
η	– overall heat transfer coefficient

Subscripts

c	– corrugated tube
i, j, k	– direction of co-ordinate
t	– turbulence
s	– smooth tube
w	– tube wall

Acknowledgment

The authors gratefully acknowledge the support by the National Natural Science Foundation of China (Grant No. 51506034).

References

- [1] Wen M. Y., Flow Structures and Heat Transfer of Swirling Jet Impinging on a Flat Surface with Micro-Vibrations, *International Journal of Heat and Mass Transfer*, 48 (2005), 3-4, pp. 545-560
- [2] Das, S. S., *et al.*, Mass Transfer Effects on MHD Flow and Heat Transfer Past a Vertical Porous Plate through a Porous Medium under Oscillatory Suction and Heat Source, *International Journal of Heat and Mass Transfer*, 52 (2009), 25-26, pp. 5962-5969
- [3] Fujii, K., Yamada, M., Enhancement of Melting Heat Transfer of Ice Slurries by an Injection Flow in a Rectangular Cross Sectional Horizontal Duct, *Applied Thermal Engineering*, 60 (2013), 1-2, pp. 72-78
- [4] Lu, J. F., *et al.*, Convective Heat Transfer of High Temperature Molten Salt in Transversely Grooved Tube, *Applied Thermal Engineering*, 61 (2013), 2, pp. 157-162
- [5] Zheng, N. B., *et al.*, Heat Transfer Enhancement in a Novel Internally Grooved Tube by Generating Longitudinal Swirl Flows with Multi-Vortexes, *Applied Thermal Engineering*, 95 (2016), Feb., pp. 421-432
- [6] Han, H. Z., *et al.*, Numerical Study of Flow and Heat Transfer Characteristics in Outward Convex Corrugated Tubes, *International Journal of Heat and Mass Transfer*, 55 (2012), 25-26, pp. 7782-7802
- [7] Van Rooyen, R. S., Kroeger, D. G., Laminar Flow Heat Transfer in Internally Finned Tubes with Twisted-Tape Inserts, *Proceedings*, 6th IHTC, Toronto, Canada, 1978, Vol. 2, pp. 577-581
- [8] Pramanik, D., Saha, S. K., Thermohydraulics of Laminar Flow through Rectangular and Square Ducts with Transverse Ribs and Twisted Tapes, *ASME Journal of Heat Transfer*, 128 (2006), 10, pp. 1070-1080
- [9] Bharadwaj, P., *et al.*, Heat Transfer and Pressure Drop in a Spirally Grooved Tube with Twisted Tape Insert, *International Journal of Heat Mass Transfer*, 52 (2009), 7-8, pp. 1938-1944
- [10] Liao, Q., Xin, M., Augmentation of Convective Heat Transfer Inside Tubes with Three-Dimensional Internal Extended Surfaces and Twisted-Tape Inserts, *Chemical Engineering Journal*, 78 (2000), 2-3, pp. 95-105
- [11] Promvongse, P., Eiamsa-ard, S., Heat Transfer Behaviors in a Tube with Combined Conical-Ring and Twisted-Tape Insert, *International Communication in Heat and Mass Transfer*, 34 (2007), 7, pp. 849-859
- [12] Hong, M. N., *et al.*, Compound Heat Transfer Enhancement of a Converging-Diverging Tube with Evenly Spaced Twisted-Tapes, *Chinese Journal of Chemical Engineering*, 15 (2007), 6, pp. 814-820
- [13] Thianpong, C., *et al.*, Compound Heat Transfer Enhancement of a Dimpled Tube with a Twisted Tape Swirl Generator, *International Communication in Heat and Mass Transfer*, 36 (2009), 7, pp. 698-704
- [14] Yakhot, V., Orszag, S. A., Renormalization Group Analysis of Turbulence, I. Basic Theory, *Journal of Scientific Computing*, 1 (1986), 1, pp. 3-51
- [15] Manglik, R. M., Bergles, A. E., Heat Transfer and Pressure Drop Correlations for Twisted-Tape Inserts in Isothermal Tubes – Part II: Transition and Turbulent Flows, *ASME Journal of Heat Transfer*, 115 (1993), 4, pp. 890-896